Biosensors and Bioelectronics 144 (2019) 111693

Contents lists available at ScienceDirect

Biosensors and Bioelectronics

journal homepage: www.elsevier.com/locate/bios

Optical biosensors based on refractometric sensing schemes: A review

Yangyang Chen[a,b], Jinchuan Liu[a], Zhenchuan Yang[b], James S. Wilkinson[c,*], Xiaohong Zhou[a,d,**]

[a] State Key Joint Laboratory of ESPC, School of Environment, Tsinghua University, Beijing, 100084, China
[b] National Key Laboratory of Science and Technology on Micro/Nano Fabrication, Institute of Microelectronics, School of Information Science and Technology, Peking University, Beijing, 10084, China
[c] Optoelectronics Research Centre, Southampton University, Highfield, Southampton, SO17 1BJ, UK
[d] National Engineering Laboratory for Advanced Technology and Equipment of Water Environment Pollution Monitoring, Changsha, 410205, China

ARTICLE INFO

Keywords:
Guided-wave optical biosensor
Label-free biosensing
Refractive index
Applications

ABSTRACT

Biosensor technology is an active field of research and development presenting rapid progress in recent decades, and the subfield of optical biosensors based on refractometric sensing schemes has developed dramatically during this time. This review focuses on advances in the refractometric sensing-based guided-wave optical biosensors particularly in the last two decades. It starts with a concise discussion on the underlying principles of label-free refractometric biosensor. Subsequently, advances in biosensor design, especially the transducer configuration and the integration of the sensing device are reviewed, highlighting the challenges and efforts dedicated to improving this technology. Various surface functionalization strategies designed to produce well-defined and reproducible surface properties are introduced for evaluation. Refractometric sensing scheme-based optical biosensors have found versatile applications varying from environmental monitoring and food safety to clinical diagnostics, together with advances in these applications and others are described. This paper concludes with a brief discussion on the outlook for integrating biosensors with emerging technologies.

1. Introduction

Biosensors are analytical devices that incorporate a biorecognition element, which may be a biological material (e.g. enzymes, antibodies, nucleic acids, cell receptors, microorganisms, tissue, organelles and natural products), a biomimic (e.g. imprinted polymers, biomimetic catalysts, synthetic receptors and combinatorial ligands) or a biologically derived material (e.g., functional nucleic acids, recombinant microorganisms, engineered proteins) and these materials, which provide biochemical specificity, are in intimate association or integration within a physicochemical transducer, which may be electrochemical, optical, magnetic, thermometric, piezoelectric or micromechanical (Turner, 2013; Inan et al., 2017; Jayanthi et al., 2017), and the crucial components are shown in Fig. 1. Among the various transduction approaches, optical biosensors have attained numerous attentions in the past decades as powerful detection and analysis tools with wide applications. They offer significant advantages over other well-developed technologies such as electrochemical, thermometric, piezoelectric or magnetic biosensors, including lower noise and immunity to electromagnetic interference (Damborský et al., 2016; Sadani et al., 2019). Generally, two broad classes of detection protocols can be utilized in optical biosensing, namely label-based and label-free detection. Comparatively speaking, targeted biomolecules are detected closer to their natural forms as they are not altered by labelling in label-free detection. Thus the label-free detection is not only facile and inexpensive to perform, but also allows undisturbed kinetic measurements of molecular interactions and target quantification. With the continuous efforts recently years, some label-free optical transducers can even achieve a single molecule detection as well (Baaske et al., 2014).

Refractive index (RI)-based label-free optical biosensing is by far the most successful and commonly used approach to date and such biosensors are utilized for a wide range of applications because of their excellent performance, ease of use and low cost. They also have great potential for miniaturization and for simultaneous multiplexed detection of multiple analytical targets (Kozma et al., 2014). While recent detailed reviews of the optical performance of refractometric biosensors have been published (Vollmer and Yang, 2012; Xavier et al., 2018), the surface chemistry and mode of application are at least as important as the optical performance. The physical transduction element cannot be considered in isolation from the biorecognition element and the practicalities of real samples, and the biosensor designer needs to understand the interrelationship of these three elements to design a complete

* Corresponding author. Optoelectronics Research Centre, Southampton University, Highfield, Southampton, SO17 1BJ, UK
** Corresponding author. State Key Joint Laboratory of ESPC, School of Environment, Tsinghua University, Beijing, 100084, China.
E-mail addresses: jsw@soton.ac.uk (J.S. Wilkinson), xhzhou@mail.tsinghua.edu.cn (X. Zhou).

https://doi.org/10.1016/j.bios.2019.111693
Received 10 July 2019; Received in revised form 30 August 2019; Accepted 6 September 2019
Available online 11 September 2019
0956-5663/

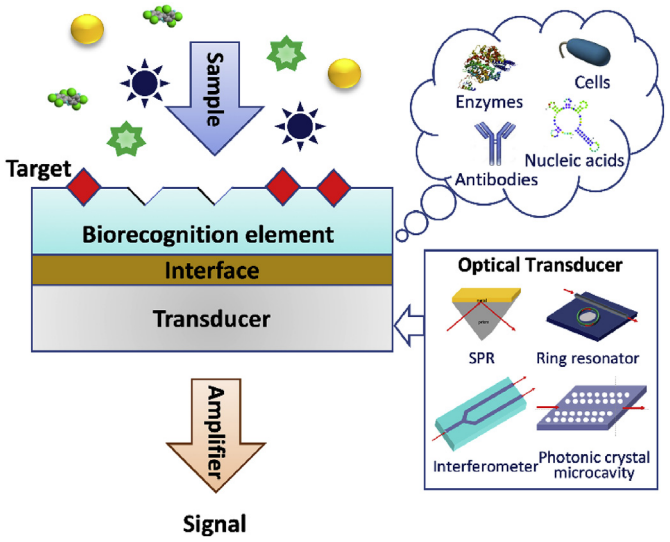

Fig. 1. Schematic diagram of biosensor constitution. Inserts show the typical biorecognition elements and optical transducers for label-free refractometric biosensing with modification from Ref. (Kozma et al., 2014).

system with good sensitivity and selectivity. To the best of our knowledge, complete refractometric biosensors including optical transducer, surface chemistry and application have not been comprehensively reviewed in the literature so far. This review presents a systematic and comprehensive summary of refractometric sensing-based guided-wave optical biosensors, predominantly over the last two decades, describing optical approaches for enhanced sensitivity, compactness and integration, biofunctionalization methods for highly chemical specificity and exemplar applications in terms of different biological recognition materials.

2. Refractometric optical transducers and instrumentation

Refractometric optical biosensors exploit the phase change caused by the product of a change in RI (or effective RI) and the propagation length (or effective propagation length). Overview of principles, including sensitivity and limit of detection (LoD), evanescent wave transduction and optical waveguides as transducers, are introduced in Supplementary Information, Note S1.

In the following subsections, several guided-wave refractometric transducers using evanescent wave interrogation and their instrumentation are described, drawing upon these basic waveguide concepts.

2.1. Non-resonant interferometer-based biosensors

Ultimately, all refractometric biosensors exploit a form of interference to transform a phase change into an intensity change. The Mach-Zehnder Interferometer (MZI) and the Young Interferometer (YI) are the most common and straightforward non-resonant examples as shown in Fig. 2. Both configurations separate a light beam into two independent waveguide paths and recombine them together either on-chip (in the case of MZIs) or via free space on an image sensor (in the case of YIs). One path is not exposed to the target materials and acts as a reference while, in the other path, variations in the waveguide n_{eff} along the area of sensing due to variations in surface film RI are directly converted into changes in the output power (in the case of MZIs) or shifting fringes (in the case of YIs). In both cases the waveguide itself is optimized by maximising the change in n_{eff} with thickness or RI of a thin surface biorecognition layer at the waveguide surface, which corresponds to maximising the modal surface intensity for given modal power. The sensing region is normally defined by depositing a low-index cladding over the rest of the sensor chip.

2.1.1. The Mach-Zehnder Interferometer (MZI)

MZIs are the most extensively exploited interferometric transducers. The incident monochromatic light at the input of an MZI-based biosensor is split into two arms by a Y-junction. The binding interaction between the biorecognition element specially functionalized on the sensing area and target locally alters the effective index of refraction, and hence is "probed" by the evanescent wave of the guided mode. Thereby, it results in a phase change between both propagating beams that can be directly converted into changes in the output power recorded by an optical device such as a photodetector (Fig. 2a).

In the MZI, the phase difference between both of the arms is described as follows (Kozma et al., 2014):

$$\Delta\phi(t)_{MZI} = \frac{\partial\phi}{\partial n_{eff}}\frac{\partial n_{eff}}{\partial n_c}\Delta n_c + \frac{\partial\phi}{\partial n_{eff}}\frac{\partial n_{eff}}{\partial d_A}\Delta d_A = k_0 L S_c \Delta n_c + k_0 L S_A \Delta d_n, \tag{2.1}$$

and the power received at the detector is given by:

$$P_{out}(t) = \frac{P_{in}}{2}[1 + \cos(\Delta\phi(t)_{MZI})], \tag{2.2}$$

where P_{in} is the waveguide input power, L is the waveguide length exposed to the biorecognition material, n_{eff} is the effective indices of the sensing path. Heideman et al. (1991) first demonstrated the potential of Mach-Zehnder interferometry as a biosensing device. This sensor exhibited a detection of human chorionic gonadotropin (hCG) as low as 2.5×10^{-8} M. An improved version of this system using the same waveguide configuration, but with etched gratings to provide both optical in- and out-coupling of the waveguide modes, was demonstrated to a reduced LoD down to 5×10^{-11} M (Heideman et al., 1993). In addition to such silicon-compatible materials, polymers are competitive for their cost effectiveness and simple fabrication processes. SU-8 resist is the material most commonly used to realize polymeric interferometric waveguides wherein the RI can be tuned to a certain extent through UV exposure. Polyimide (n = 1.50–1.76 at λ = 633 nm) is also a typical polymeric material acting as a core layer (Melnik et al., 2011) which shows well transparent at the desired wavelength, strong chemical resistance and high RI, avoiding the minimal surface sensitivity of MZI biosensors made by polymer with limited range of refractive indices. During the continuing devotion to enhance the sensitivity of MZI-based biosensors, the slot waveguides have been used in the sensing arm due to its stronger overlap of the modal field with surface films and increased reaction surface area, which combine to strengthen the light-target interaction and further increase sensitivity. The bulk RI sensitivity of the MZI sensor with a slot waveguide arm in 7 mm length exhibits an improved sensitivity of 1864 π/RIU higher than 865 π/RIU of the conventional Si_3N_4-based MZI device (Liu et al., 2013). Further to improving sensitivity, advances are being made in integrating sensors in designs for point-of-care (POC) applications. Such integration approaches have included integrating MZIs with other optical devices such as lasers and photodetectors on a chip and integrating several MZIs together to realize multisensing or high-throughput detection in Fig. 2c, which reduces the size of the sensor system and decreases the measurement time in comparison with monitoring each target individually (Liu et al., 2015a).

2.1.2. The Young Interferometer (YI)

In contrast to the MZI biosensor structure, a YI-based biosensor lacks the second Y-junction to recombine the beams of light from two arms. Instead, light from the reference and sensing waveguide ends diffracts and interferes on an image sensor (e.g. a charge-coupled device (CCD), camera) to create interference fringes. Variations in the effective RI due to biomolecular binding in the sensing area are directly translated into shifting fringes on the image sensor (Fig. 2b). The integrated YI biosensor was first demonstrated to use the waveguide with high-RI

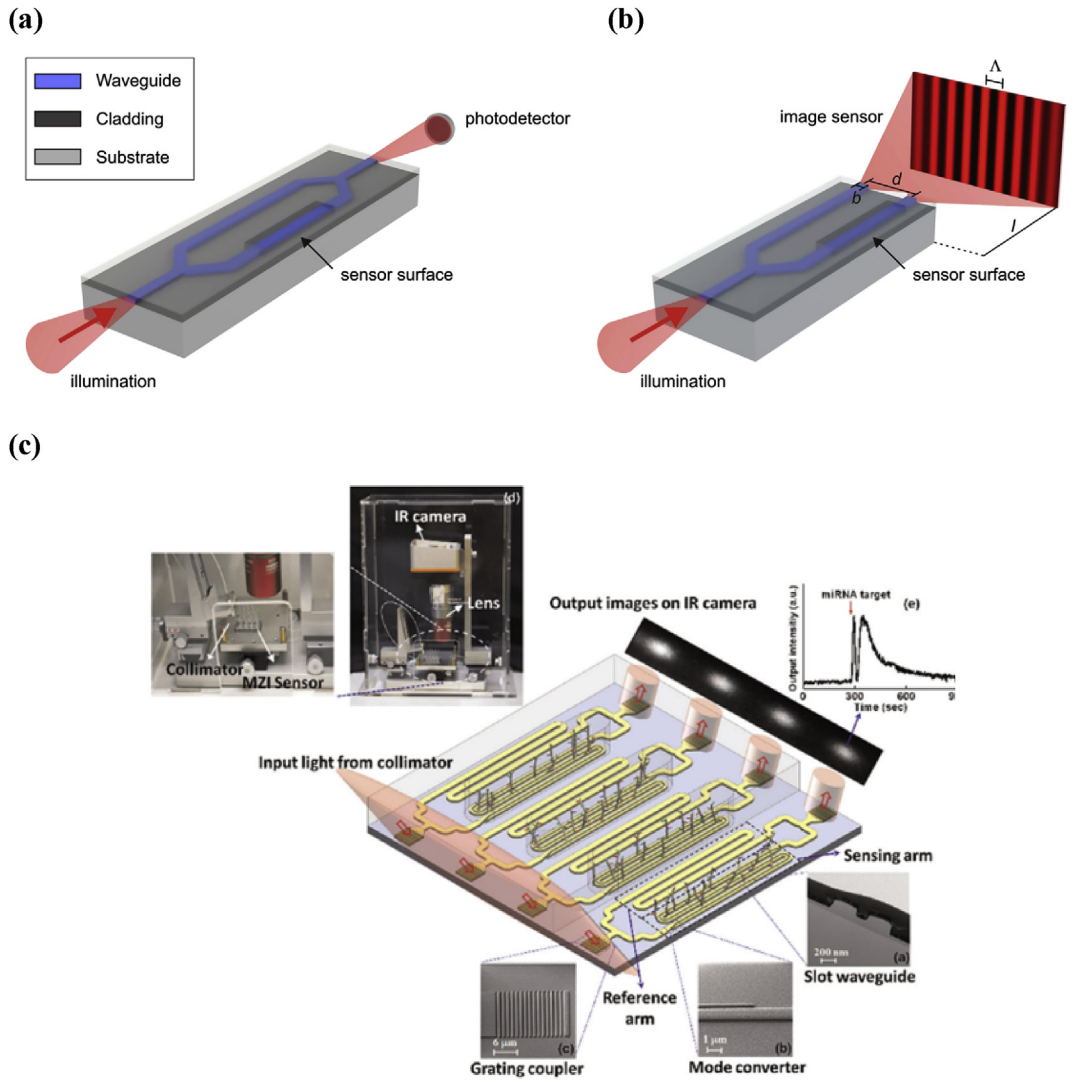

Fig. 2. Schematic of **(a)** MZI and **(b)** YI configurations (Reprinted from (Kozma et al., 2014) with permission); and example of **(c)** integrated MZI biosensor system for detecting miRNA (reprinted with permission from Ref (Liu et al., 2015a)), which consists of four identical MZI sensors for multiplexed detection of miRNA in a single reaction. For each MZI sensor, a strip waveguide acts as the reference arm (1 μm in width, 400 nm in thickness with a 75 nm thick slab), however a slot waveguide acts as the sensing arm (500 nm in width, 75 nm in thickness of slab with a 200 nm wide gap).

films deposited on oxidized silicon wafers and reported to have a RI resolution of 1.43×10^{-6} (Brandenburg et al., 2000). Multiplexed detection was proposed using a four-channel integrated YI sensor with the ability to simultaneously monitor three biomolecule binding processes, showing that a specific and sensitive monitoring of samples down to a low concentration (850 HSV-1 particles/mL) (Ymeti et al., 2007).

The YI biosensor has the advantages over the simple MZI that (i) there are no regions of zero sensitivity as occur for integer multiples of π radian phase difference in the MZI (ii) ambiguity in the direction of change of phase is eliminated and (iii) the structure is more compact for multiplexed detection as only one reference branch is needed for multiple sensing branches. Interferometer-based biosensors such as the MZI and YI are popular given their simplicity and ease of fabrication. However, it is difficult to miniaturize the sensing area without losing sensitivity, so that multipass or resonant approaches may be preferred where small footprint and ultralow sample volume are required, if the LoD × surface area product can be reduced.

2.2. Surface plasmon (SP) based biosensors

SPs are electromagnetic excitations which propagate along a interface between the dielectric medium and metal, and SPs comprise charge density oscillations in the metal and an evanescent wave bound to the interface in the dielectric medium (Wijaya et al., 2011). For the purposes of biosensing they are similar to waveguide modes, having an evanescent field in which a change in bulk or thin film RI induces a change in the velocity of the SP. The principal difference from dielectric waveguides modes is that SPs are intrinsically very absorptive due to the optical absorption of the metal, so that no specific interference technique needs to be used to translate velocity changes into intensity changes. Instead, usually, resonant coupling to the SP from an incident wave is used so that RI-induced changes in the SP velocity result in detuning of the coupling into the SP and a resultant reduction in absorption. A change in the RI in the evanescent field induces a variation in the "resonant" angle, and it is this which leads to the term SP resonance (SPR). Basic principle of SP, coupling methods to excite SPs and resonance conditions are introduced in Supplementary Information, Note S2.

2.2.1. SPR, SPR imaging (SPRi) and SPR microscopy (SPRM)

Conventional SPR system based on prism coupling has been extensively studied and maturely commercialized, showing a RI resolution of approximately 10^{-6} RIU (Suzuki et al., 2005). Building on the basic structure of SPR, sensitivity enhancement can be achieved by: (i) optimizing the SPR-carrying layer, (ii) adding a nanodielectric layer, and (iii) utilizing phase modulation. The width of the reflectance dip, and thus sensitivity to small RI changes, is affected substantially by absorption in the metal layer. Therefore, optimizing SPR-carrying layers can be achieved by selecting different metal materials and optimizing their thicknesses. Silver (Ag) and gold (Au) are noble metals with a small imaginary part of permittivity that reduces the dissipation and consequently obtains a narrow dip in reflectance angle or spectrum. Ag possesses better optical properties at visible and NIR wavelengths than Au but suffers from low chemical stability, so that Au is more often chosen. Fig. S5 illustrates different materials, structures, and applications reported for SPR-based biosensors.

Nanomaterial layers have been extensively utilized for improving the sensitivity of SPR-based biosensors. Graphene was proposed to enhance the sensitivity of SPR sensor given the increasing biomolecule adsorption on the SPR sensor surface (Wu et al., 2010). The heterostructures of few-layer black phosphorus (BP) and 2D nanomaterials (e.g. graphene/transition metal dichalcogenides) are utilized to amplify the signal of SPR. On the basis of the angular interrogation, the highest sensitivity attained to be 279°/RIU once the heterostructure of bilayer WSe2 and BP was used, thereby improving sensitivity for approximately 2.4 times over a conventional SPR with only single Ag film (Wu et al., 2017).

Fixed wavelength, fixed angle intensity interrogation suffers from low sensitivity and resolution due to noise and drift. At SPR, the phase of the reflected light changes rapidly on passing through resonance and this, combined with interferometry, can be used to achieve more sensitive operation. The “probe” beam is p-polarised and excites the SP while the “reference” beam is s-polarised and does not. Maximal phase variation with RI occur at the minimum of the SPR response curve, whereas the maximum of amplitude changes exist on the resonance slopes (Liu et al., 2017). Hence, the phase sensitivity to RI changes is at least 100 times higher than the amplitude sensitivity to RI variations (Kabashin et al., 2009). The phase modulation approach is well-suited to SPRi and multiplex analysis of thousands of channels in parallel (Piliarik et al., 2010). SPR interferometry, SPR polarimetry, and optical heterodyne are three strategies in the SPR biosensor to realize a phase sensitive detection. Various configurations and schemes for the SPR-phase detection can be found in previous review paper (Mohammadzadeh-Asl et al., 2018).

Other approaches to enhancing the performance of SP based biosensors, beyond adopting new interrogation methods, exploit changing the structure of conventional SPR devices or the instrumentation, including: (i) SPRi with arrayed reaction areas and CCD camera detection enabled high-throughput detection; (ii) SPRM, utilizing a high numerical aperture (NA) lens for light coupling has resulted in high resolution detection and single-molecule analysis; and (iii) Long range SPR (LRSPR), where a thin film of metal, typically 20–25 nm, is used and the resulting low propagation loss and deeper field penetration of LRSPR increases sensitivity and LoD for detection of large targets. Comparison of three types of SPR configuration, SPR, SPRi and SPRM are presented in Fig. 3a. SPRi uses the same detection principle as SPR with additional spatial imaging for high-throughput assay by using a CCD array as a detector and is typically conducted at a fixed incident angle. The distribution of reflected light intensity depends upon from molecular concentrations distributed on the different regions of the sensing surface. Numerous reviews can be found on SPRi biosensors, such as Ref. (Liu et al., 2017).

However, conventional SPRi, using the prism configuration, has inherently limited NA and magnification ratio of an imaging system, thereby providing poor spatial resolution. An alternative approach, so-called SPRM, has been developed recently, offering spatial resolution close to the diffraction limit (Jamil et al., 2008; Yu et al., 2017). SPRM consists of an inverted microscope and an oil immersion objective with high NA. The high sensitivity has enabled it successfully exploited in several critical applications, such as optical mapping and a single-molecule analysis.

The optical penetration depth limits application of SPR in detecting bacteria and cells, several cell-based assays have been exhibited. In order to increase the sensitivity in detection of large targets such as bacteria and cells, LRSPR has been developed. LRSPR utilizes a very thin film of metal inserted into two dielectric materials with very close refractive indices, one of which is the target (Fig. 3b). This provides two advantages: (i) the evanescent penetration depth is larger than in conventional SPR, resulting in better overlap with large targets and (ii) the propagation loss is lower, resulting in a narrower resonance dip and thereby improving the resolution of the sensor. An LRSPR biosensor to detect *E. coli* HB101P was developed with a sensitivity 2.5–5.5-fold greater than the conventional SPR biosensor, showing a sensitivity to bulk RI changes of 5.9×10^4 nm/RIU and resolution of 5×10^{-8} RIU (Vala et al., 2009).

2.2.2. Localized SPR (LSPR)

When an SP is confined to a conductive nanoparticle (NP) with a size comparable to (or smaller than) the light wavelength, the free electrons of NP involve in collective oscillation, resulting in the localization of the SP to the NP (Mayer and Hafner, 2011). The resonant frequency of such localized plasmon oscillations strongly depends on the size, composition, dielectric environment, geometry, and the extent of aggregation of NPs. At resonance, the electric fields close to the NP surface are greatly enhanced and decay very fast with the distance away from the surface. The optical extinction of NPs reaches the maximum at the frequency of plasmon resonant given at the wavelengths of visible light for noble metal NPs. The highly localized and extremely intense electromagnetic fields induced by LSPR enable NPs be highly sensitive transducers to sense small variations in the local RI. These variations are shown in the scattering spectra and the spectral shifts of extinction (absorption plus elastic light scattering) (Fig. 3c). For organic-molecular targets with a RI higher than the target matrix, the event of binding to NPs leads to a red shift of the resonances, which can be monitored to quantify the binding event in a similar way as SPR. There are two key differences, however, which make LSPR attractive for biosensing: (i) the evanescent field decays away from the NP 10-100 times more rapidly than in conventional SPR, leading to reduction in interference from background matrix changes including temperature and (ii) in contrast to SPR, LSPR does not require the use of prisms or waveguides for phase-matching to a propagating mode, so that the extinction spectrum of assemblies of NPs can be monitored by direct illumination and the approach may be more cost-effective and easier to miniaturize (Svedendahl et al., 2009).

Mie theory is used to give the extinction spectrum for small well-dispersed NPs (Link and El-Sayed, 1999)

$$C_{ext} = \frac{18\pi V \varepsilon_m^{3/2} N}{\lambda \ln(10)} \frac{\varepsilon_i}{(\varepsilon_r + \chi\varepsilon_m)^2 + \varepsilon_i^2}, \tag{2.3}$$

where C_{ext} is the extinction cross-section, ε is the complex dielectric constant of the bulk metal ($\varepsilon = \varepsilon_r + i\varepsilon_i$), ε_m is the dielectric constant of the surrounding medium, V is the volume of the NP and N is the number of NPs per unit volume. The factor χ is associated with the shape of the NP, which is designated a magnitude of 2 for a spherical NP and even up to 20 for NPs with relatively high aspect ratios. For metals with negative permittivity, which support SPs, the term $(\varepsilon_r + \chi\varepsilon_m)^2$ equals zero at the resonant wavelength, giving rise to a strong peak in extinction.

The relationship between the RI of the medium n_m and the LSPR peak (resonance) wavelength λ_{max} is given by (Mayer and Hafner,

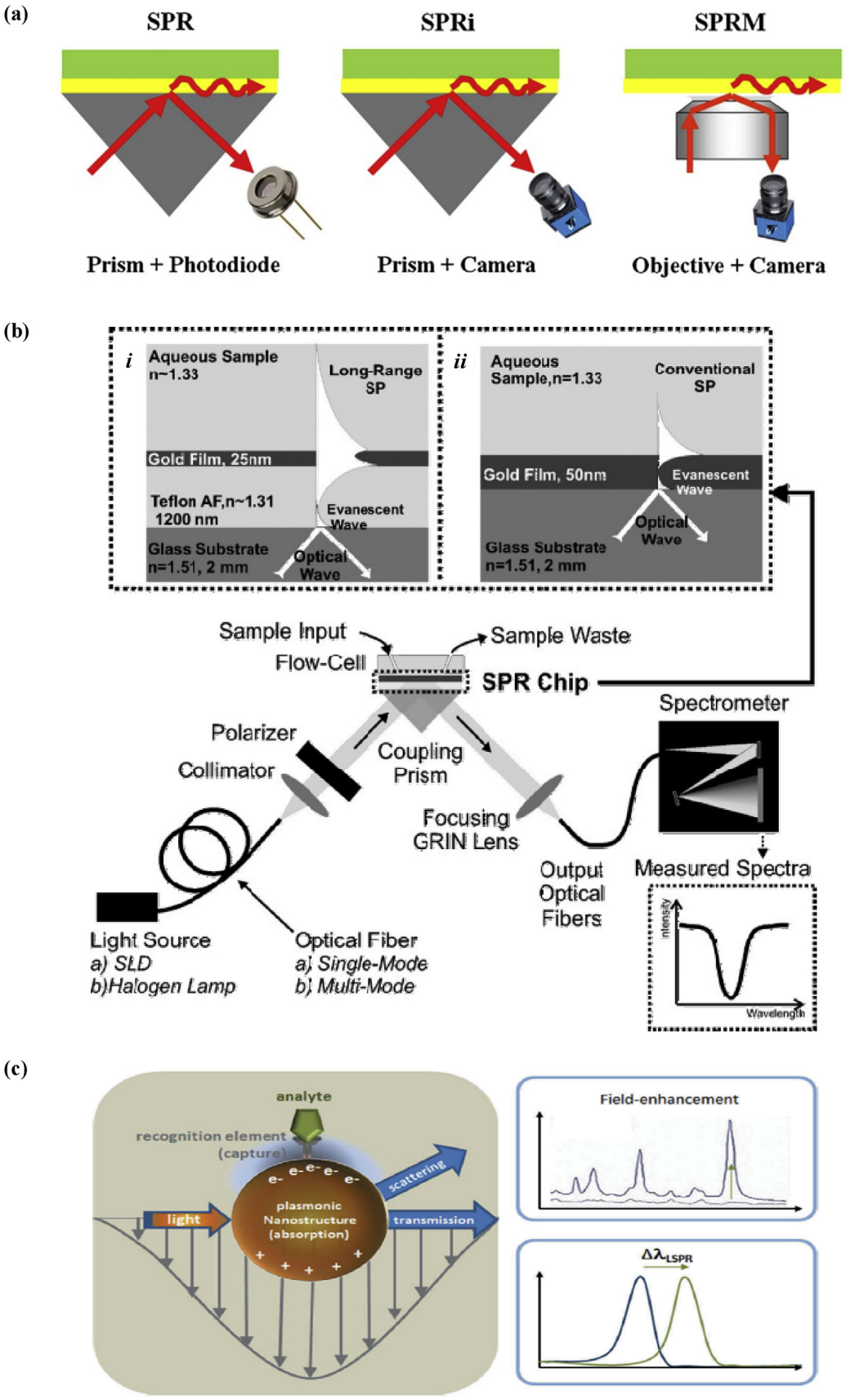

Fig. 3. (a) Three types of SPR configuration. In SPRi, the introduction of a camera adds imaging capability and enables high-throughput detection. In SPRM, replacing the prism with a high NA oil immersion objective enhances spatial resolution (reprinted with permission from Ref (Su and Wang, 2018)); **(b)** Comparison of two types of SPR structures: *i*) LRSPR consisting of coupled surface plasma waves on opposite sides of a thin film of metal existed between two dielectrics with very close RIs (the RI of aqueous sample ≈1.33 and the RI of Teflon AF ≈ 1.31). *ii*) Conventional SPR consisting of a BK7 glass substrate covered with 1.5 nm Ti and 50 nm Au. (reprinted with permision from Ref (Vala et al., 2009)); **(c)** Scheme of the physical effects involved in LSPR-based biosensing (reprinted with permision from Ref (Csaki et al., 2018)).

2011)

$$\lambda_{\max} = \lambda_p \sqrt{\chi n_m^2 + 1}\,, \tag{2.4}$$

where λ_p is the wavelength corresponding to the plasma frequency of the bulk metal, thereby indicating that the LSPR peak wavelength is approximately linear with the RI of the medium n_m. Thus absorption spectroscopy of a densely-packed assembly of NPs on a surface can be used to perform refractometry in a similar way to wavelength-interrogated SPR. Ultimately, as Svedendahl et al. have shown the wavelength response and surface RI behavior of SPR and LSPR are very similar but with no requirement for a prism coupler and with much greater discrimination (~20 times) against bulk matrix effects (Svedendahl et al., 2009).

LSPR biosensors exploit metal nanostructures including spheres (Xie et al., 2014), triangles (Zhao et al., 2014), and rectangles (Lee et al., 2018) as the sensing element. The peak wavelength shifts in the NP extinction and scattering spectra depend strongly on the composition and shape of nanostructures, which are associated with different χ in Eqn (2.3) (Traci R. Jensen et al., 2000). LSPR is endowed with a larger specific surface area in comparison with the continuous thin films, therefore supporting target binding to the metals and changing the measured resonances even at very small concentrations (Caucheteur et al., 2015). Five kinds of Au nanorods with different aspect ratios were used to develop a five-channel multiplexed LSPR biosensor (Huang et al., 2009). Distinct LSPR resonant peaks corresponding to each aspect ratio allowed different pairs of acceptor–ligand to be monitored at the same time over the wavelength range of 530–940 nm using a conventional spectrometer. Studies on performance enhancement methods target optimum choice of material and geometry of NPs are introduced in Supplementary Information, Note S3. The combination of two dimensional (2D) nanomaterials (i.e. graphene and graphene oxides) with plasmonic metal NPs to design the LSPR biosensing system is providing new and exciting opportunities. The graphene-based 2D nanomaterials can enhance local electromagnetic fields and facilitate the surface functionalization with many biorecognition materials owing to their capabilities to bind with the aromatic-ring amino acids of proteins via π-π interaction, it (Chiu et al., 2018; Ng et al., 2017). Whilst ionic poly(N-isopropylacrylamide-co-methacrylic acid) (PNM) hydrogel was utilized as a protein receptor owing to the large increase in refractive index once binding protein with a sensitivity of 210 nm/RIU (Culver et al., 2018).

2.3. Whispering-gallery mode (WGM) biosensors

WGM microcavities and the closely related ring resonators use low-loss dielectric materials, in common with MZIs and YIs, but use a re-circulating path to produce wavelength resonances through internal interference, rather than by using a lossy metal (Nordin, 2016). This results in much sharper wavelength “dips” than SPR and LSPR, due to the minimization of absorption (high quality factor). While the basic sensing phenomenon is the same in each case – a change in RI within the evanescent field alters the light velocity and hence the phase delay with distance – the sharpness of the resonances means that changes in resonant wavelength can be monitored with higher resolution. This enhanced light-matter interaction provided by WGM and ring microcavities can support high surface RI resolution in a small area with robust wavelength interrogation. The diameter (and hence round-trip pathlength) of an WGM or ring resonator is normally small (microns rather than millimetres), allowing biosensing in small areas with small volumes. This leads to a small phase change for biomolecule binding on the resonator surface *per round-trip* but this is compensated by the much greater sharpness of the resonances. This may be quantified by considering that, in contrast to other types of biosensors, WGM-based biosensors allow light to recirculate many times building up the evanescent interaction with the target over a much greater effective path length, expressed as follows:

$$L_{eff} = \frac{Q\lambda}{2\pi n_{eff}}, \tag{2.5}$$

where the n_{eff} is the effective RI of the WGM, λ is the resonant wavelength, and Q, the quality factor (Q-factor), is calculated by cavity loss mechanisms and given by (Gorodetsky et al., 1996);

$$\frac{1}{Q} = \frac{1}{Q_{rad}} + \frac{1}{Q_{abs}} + \frac{1}{Q_{sac}}, \tag{2.6}$$

Where Q_{rad} is the radiative loss because of the resonator curvature, Q_{abs} is the material absorption loss in the resonator (including the evanescent region), and Q_{sac} is the surface scattering loss. The resonance spectral line width, $\delta\lambda$, is then correlated to Q as follows:

$$Q = \frac{\lambda}{\delta\lambda}, \tag{2.7}$$

High Q-factor is achieved by using a material with low absorption, a fabrication approach with low surface roughness and a sufficiently large resonator diameter. In principle, WGM resonator resolution may be most easily compared that of with MZI and YI sensors using L_{eff} and with SPR sensors using $\delta\lambda$. In the latter case the capability to measure small shifts in the wavelength of resonance is improved due to the spectrally narrow resonances as a result of high Q.

2.3.1. Microsphere resonators

The paradigm for WGM resonators is a glass microsphere resonator which typically has a quality factor of $> 10^5$ with a diameter of a few tens of microns (Foreman et al., 2015). Fig. 4a–c illustrates the operation of WGM sensors, with Fig. 4c showing that how a tapered optical fiber is used to couple light in and out. In this case the Q value of the microsphere was 6.4×10^5 and it was used to detect influenza A virus particles (Vollmer et al., 2008). Although microspheres are easy to fabricate, stable coupling with a tapered fiber is difficult in a practical device and the potential for integration for multiplexing is limited, leading to the pursuit of circular resonators fabricated on robust planar substrates.

2.3.2. Planar microring resonators

Planar microring resonators are robust and suitable for multiplexing and integration with microfluidics due to their optical coupling via waveguide instead of tapered fibers used in microspheres (Kim et al., 2017). Moreover, they are compatible with conventional semiconductor fabrication techniques, thus facilitating mass production. However, conventional planar ring resonators are limited by their poor detection sensitivities, having Q values in the range of 10^4-10^5 due to the light loss leaking into the underlying substrate and absorbed by water in infrared region (Hu et al., 2017). The incorporation of a slot waveguide in a ring resonator biosensor has been pursued for the performance optimization because the circulating light can be concentrated strongly inside the slot and thereby interact strongly with the target (Claes et al., 2009). Taniguchi et al. demonstrated a LoD of approximately 1×10^{-8} g/mL prostate-specific antigen using a Si_3N_4 slot-ring biosensor (Taniguchi et al., 2016).

A ring resonator sensor using a 5 μm-radius double-slot waveguide was also demonstrated on a SOI platform to further improve the sensitivity, achieving a sensitivity of 708 nm/RIU (Yuan et al., 2014). A cascaded double-microring resonator comprising two similar microring resonators cascaded however with different radii was proposed as shown in Fig. 4d. This uses the Vernier effect to enhance sensitivity and avoid utilizing a high-resolution optical spectrometer (Luo et al., 2014). A LoD of 7.1 μg/mL has been obtained for human immunoglobulin G using a cascaded double-microring resonator (Chen et al., 2015b).

Subwavelength grating waveguides (SWG) are also effective for enhancing a ring resonator's sensitivity and decreasing the LoD. In an SWG ring resonator sensor, periodic silicon pillars largely smaller than

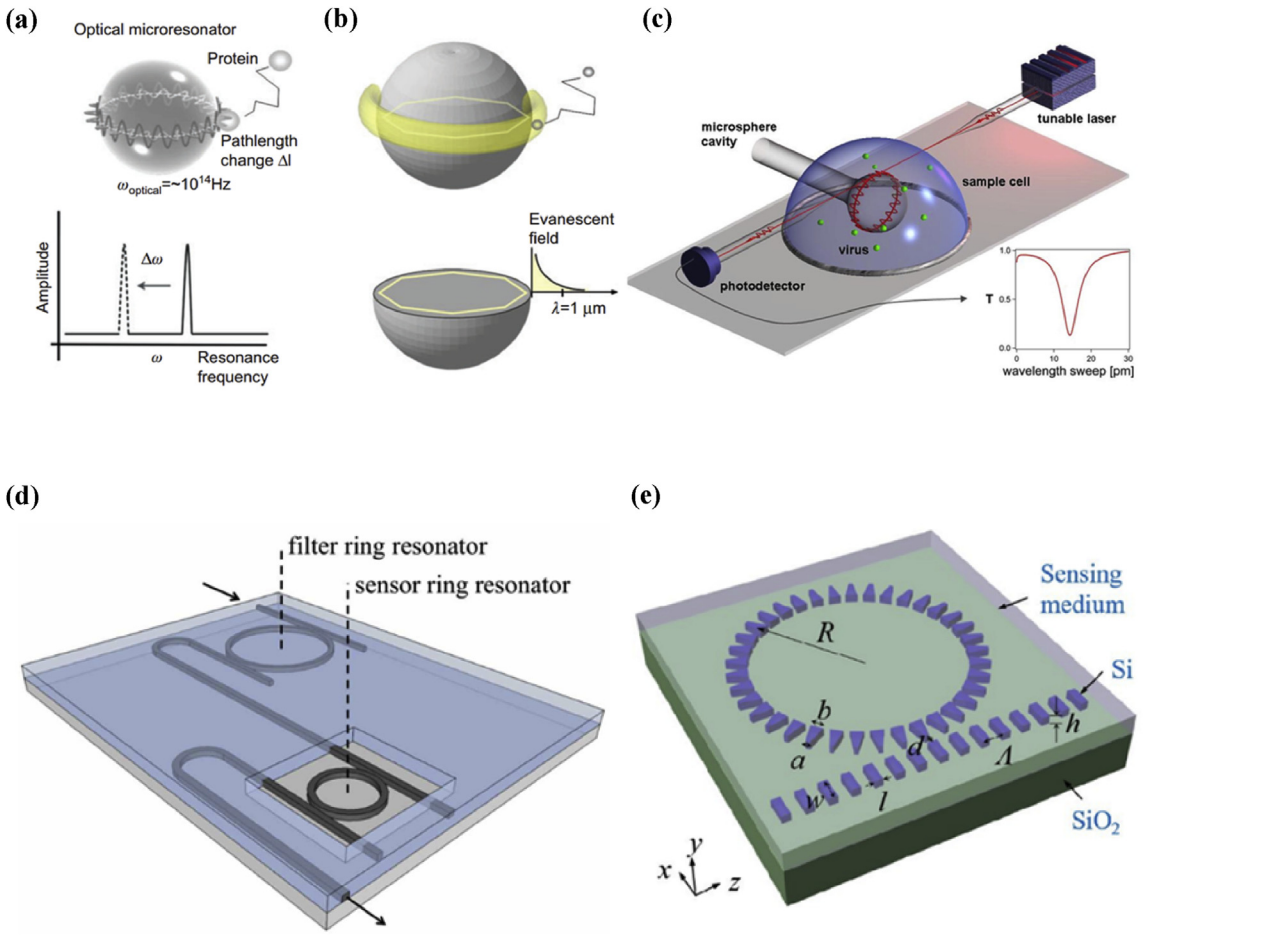

Fig. 4. (a) Illustration of whispering gallery modes (WGM) in glass microspheres. A protein binding event with the microsphere surface enables the increased WGM path length, which can be monitored as a shift in the resonance frequency. **(b)** The binding of molecular to the microsphere surface is within the evanescent field of a WGM (highlighted by yellow ring). (reprinted from Ref (Vollmer and Yang, 2012). with permission) and **(c)** an example of single virus detection using an equatorial WGM of a microsphere through evanescent coupling into a guided wave in a tapered fiber (reprinted with permission from Ref (Vollmer et al., 2008)). **(d)** Illustration of the concept of cascaded double-microring resonator biosensor working analogously to a Vernier-scale. Both of microring resonators with different radii are cascaded. A thick cladding is used to cover the complete chip, only leaving a sensing area on one of the resonators, i.e. the sensor ring resonator. It is exposed to its environment and senses to the RI variations, whilst the filter ring resonator is isolated from the RI variations due to the cladding (reprinted with permission from Ref (Claes et al., 2010)). **(e)** Schematic of the SWG microring resonator biosensor comprises periodic silicon pillars with a period largely smaller than the operating wavelength along the propagation direction (grating period of the SWG is $\Lambda = 200$ nm, reprinted with permission from Ref (Yan et al., 2017)). (For interpretation of the references to colour in this figure legend, the reader is referred to the Web version of this article.)

the operating wavelength are developed along the propagation direction of the SWG ring resonator (Fig. 4e). The SWG further extends the interaction region between the cladding materials and the light compared with the conventional ring resonator. A SWG-based ring resonator was first demonstrated as a biosensor with a bulk sensitivity of 490 nm/RIU (Flueckiger et al., 2016). Sensitivity is enhanced several times higher than conventional ring resonator, but the SWG ring resonators also exhibit a large loss.

Ring resonator biosensors in materials such as porous Si and polymers are also being studied to optimize the performance of a planar ring resonator for biosensing. A ring resonator in porous Si (Rodriguez et al., 2015) exhibited a Q-factor of approximately 10000 in air and 4000 in water, a bulk sensitivity of approximately 380 nm/RIU for the detection of salt water, a surface sensitivity of approximately 4 p.m./nM and a LoD of 3 nM for nucleic acid measurement. Due to their compact size, planar ring resonators have significant potential for integration and miniaturization, leading to applications at POC for parallel multiplexed detection (Flueckiger et al., 2016) with small sample volume. Integration has allowed automation of analysis and parallel detection and relaxation of the requirements for temperature control.

2.4. Photonic crystal (PC)-based biosensors

Photonic crystals (PCs) are materials with spatially periodic RI variations leading to a wavelength band in which light is “forbidden” to propagate, in a simailar way that electrons are forbidden to possess energies in the electronic bandgap of a crystalline material (Inan et al., 2017). Defects introduced into the PC will break the periodicity of dielectric structure, resulting in narrowband defect states which providing strong confinement of EM fields, low extinction loss and small mode volume (Notomi, 2011). PC-based sensors have the potential advantages of ultra-compact size, flexibility in the configuration design, excellent sensitivity and possibility for a monolithic integration (Inan et al., 2017), so that the research on PC has been extensively carried out theoretically and experimentally. PCs are usually categorized to be 1D, 2D and 3D that depend on the numbers of periodically repetitive dimensions (Fenzl et al., 2014). 1D PCs, PC slabs, PC waveguides and PC microcavities structures are presented in Fig. S7.

Photonic crystal slabs are formed by periodical high RI slabs, which provide in-plane guided modes. RI changes on the surface of PC slabs due to the biomolecule binding events are measured by detecting the central wavelength of guided-mode resonances in a reflection or

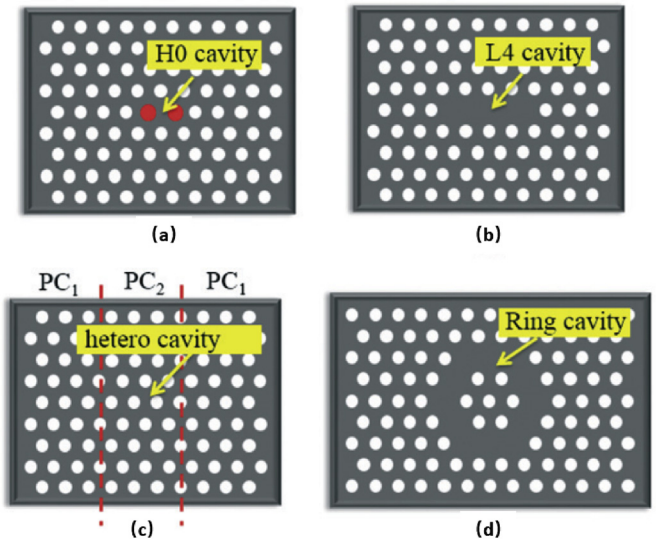

Fig. 5. Four types of PC cavities based on point defect structures: **(a)** Hm-type: changing one or more points of lattice to form a small space that is possibly encompassed with reflecting walls; **(b)** Ln-type: disappearing some points of lattice in one line to creat a cavity; **(c)** ring-type: disappearing some points of lattice to create one or more ring-typed defects and form some localized optical modes that resonated in these rings; **(d)** hetero-type: spanning numerous number of points of lattice with various constants of lattice, and holes locations, sizes, or even shapes to form resonant modes (reprinted from Ref (Zhang et al., 2017c). with permission).

transmission spectrum. PC slab sensors have been demonstrated the applications in sensing, medical diagnosis and researches, demonstrating a mass detection sensitivity of less than 1×10^{-12} g/mm^2 (Cunningham and Laing, 2006). Furthermore, the multiplexed label-free measurements on PC slab sensing platform can be achieved by using a simple CMOS camera, thus showing their potential for integration and POC application (Jahns et al., 2015). Photonic crystal waveguide (PC-WG) biosensors are formed by introducing a defect line in the lattice structure of a 2D PC. RI changes due to the molecules binding on the surface are measured by detecting the shift of a wavelength band-edge of the PC-WG biosensor. A PC-WG biosensor was developed to detect RI changes down to $\Delta n = 3 \times 10^{-3}$ (Skivesen et al., 2007). A PC microcavity is generated through bringing a point defect into the lattice structure of a 2D PC. This can be achieved by changing or removing the radius of one hole, even the radii of more holes, forming Hm-typed, ring-typed, Ln-typed and hetero-typed cavities as shown in Fig. 5 (Zhang et al., 2017c). The powerful light confinement in the PC defect cavity should result in much smaller line widths (high Qs) than other PC structures, which enhance the resolution and reduce the LoD. Microcavities with a waveguide coupling configuration have also been demonstrated, thereby allowing multiplexed detection given that the multiple cavities couple into one waveguide and measure the separate targets simultaneously with appropriate surface functionalization.

3. Surface functionalization

True biosensors generally exist in the solid state and provide a reading after contacting with the sample to be analyzed. For most biosensors, biological molecules/molecules have to be modified on the sensing transducer surface (known as receptor molecules), which serves one or more of the following functions (Wang, 2010): i) enabling semi-continuous/continuous detection of targets in flowing samples, including bioreactor fluids, blood or water samples; ii) enabling the reuse or regeneration of the biosensor; and iii) enabling the biosensor to be capable of parallel detection of multiple targets. Thus, the approach to anchore receptor molecules onto the solid sensing surface plays a crucial role in biosensor-related method, which strongly affects the analytical performance. RI-based biosensing is particularly reliant on high-quality surface functionalization to generate high-quality and repeatable interface properties and to provide high chemical specificity, rejecting non-specific interferences.

For simplicity, the receptor molecules are either chemically attached or physically absorbed onto the transducer surface. As the counterpart to physisorbed attachment with brief introduction in Supplementary Information, Note S4, chemical surface modification is generally accepted since it can create robust and stable binding between the receptor molecules and the solid surface. Besides, chemical surface modification often brings easily regenerable sensing surface using elution solutions, which can break the interaction of the receptor and its ligand and remove the ligand from the surface but not the immobilized receptor molecule itself. To remain consistent with the theme of this review, chemical surface functionalization will be summarized in relation to optical biosensors based on refractometric sensing schemes.

3.1. Metal and metal oxide

Metal material (such as gold and silver) has been widely applied for the charge density oscillations with a dielectric to construct the SPR instrument. The well-established strategy to immobilize functional groups/molecules onto thin SPR films is by using thiol-end organic compounds, which can form self-assembled monolayers (SAMs) spontaneously on metal surfaces (Thomas et al., 2018). The Au-S or Ag-S bond provides the force to anchor the compounds on the chip surface, simultaneously exposing functional group at the other end for further immobilization of bioreceptors. To fully exposed the biomolecule to the target, a series of chemical reactions are needed to covalently construct spacer arms with different lengths. The most critical technical challenge which prevents biosensors from various downstream practical applications is protein fouling. Recently, the polymer brushes functionalized with bioreceptors was used in the design of a new biointerface architecture (Blaszykowski et al., 2012) (Fig. S8), which provided excellent resistant capability against fouling from diverse and complex sample matrices including human blood plasma, urine, serum and saliva.

Tantalum oxide (Ta_2O or Ta_2O_5) is a practical material for thin-film waveguide used in the label free evanescent field sensors with high sensitivity because of low attenuation and high RI. Due to its high chemical stability, high dielectric constant and preeminent passivating properties, tantalum oxide has great potential in realizing high-quality biological interfaces (Duval and Lechuga, 2015). In the early days, the self-assembled alkanephosphate monolayers with high orientation on tantalum oxide surfaces were achieved by using bidentate and monodentate phosphate coordination to tantalum ions (Tosatti et al., 2002). This strategy is highly similar to the SAM structure on gold composed of long-chain alkanethiols. Currently, silanization is more popular used for the surface functionalization on the titanium oxide substrate due to the easy availability of silane reagents. The surface should be cleaned via piranha oxidation treatment to remove contaminations and generate reactive hydroxyl groups, which is benefit for the silane monolayer growth on the titanium oxide surface (Zhu et al., 2017). Other methods, such as oxygen plasma (Jahns et al., 2015) or UV/ozone treatment (Gunda et al., 2014) has been applied to increase the surface hydrophilicity. Given that different silane reagents are used, the silanization processes introduce amine, carboxyl, epoxy or aldehyde on the titanium oxide surface via Si-O bond, thereby enabling further covalent coupling of immobilized biomolecules effectively.

3.2. Silica glass surface

Surface functionalization of silica glass is well established by grafting the surface with the uniform reactive hydroxyl groups via piranha oxidation treatment or oxygen plasma. The following steps are

very similar to the silanization on metal oxide. By treating different silane reagents (Fig. S9), various spacer arms with different functional groups can be generated to facilitate the final covalent reactions given the diversity of receptor molecules. A generally accepted approach for surface immobilization of biomolecules (such as antibody, DNA and enzyme) on silica surface is depicted in Supplementary Information, Note S5.

3.3. Silicon-based materials

Silicon or silicon nitride materials spontaneously oxidize and form an amorphous silica layer when exposed to air. The silicon oxide layer is native and always dynamically generates on the silicon-based substrate. This native silicon oxide layer enables the standard functionalization chemistry of silica-based optical devices well suited to the silicon-based surface functionalization. Similar to the silica material, surface functionalization of silicon by covalently modifying organic monolayers has been widely explored (Bañuls et al., 2013). Most of the approaches utilize the self-assembly of a layer of organofunctional alkoxysilanes. The basis of reaction is the condensation between hyroxyl moieties on the surface and the siloxanes of the oranosilane. An example of biochemically modification of silicon substrates by utilizing the linkers of APTES and glutaraldehyde and even selective surface functionalization of a silicon nitride-based nanosubstrate is introduced in Fig. S11. Moreover, the selective surface functionalization of a silicon nitride-based nanosubstrate is introduced in Supplementary Information, Note S6.

3.4. Polymers

The employment of transparent polymers as optical waveguide materials have received numerous researches for various applications because they can be fabricated by using cost-effective fabrication technologies such as hot embossing, spin coating and injection molding, and allowing for flexible design of different configurations (Melnik et al., 2011). Recently, the bioreceptor-immobilized polymer has been developed for the recognition of target and the subsequent signal generation, exhibiting huge potential in miniaturization of bioanalytical devices and sensitivity improvement (Liu and Li, 2012). The initial step in the success of immobilizing bioreceptors on polymers is to generate the chemical functional groups on the surface such as hydroxyl (-OH), carboxyl (-COOH), amine (-NH_2) groups, and several other functional groups (e.g. carbonyl, aldehyde, thiol, silane, phosphate and hydroxyl) (Hosseini et al., 2014).

As proof of concept, Fig. 6 illustrates the most common strategy for surface immobilization of SU-8, which is a negative photoresist epoxy (Abdul-Hadi et al., 2018). The SU-8 surface is functionalized with hydroxyl groups and then silanized by immediately immersed into APTES solution. Subsequently, the aldehyde group of glutaraldehyde is combined with amine group on APTES to form an N-C bond. Finally, the covalent immobilization of bioreceptor includes the chemical reaction of amine groups on protein surface coupling on previously formed functional SAMs.

3.5. Others

Recently, numerous efforts have been devoted for the improvement of the sensitivity of refractometric sensing signals by using nanomaterials, such as Au/Ag NPs, graphene (Singh et al., 2015), graphene–MoS_2 and other hybrid nanostructures (Zeng et al., 2015). Considering dielectric confinement, sub-wavelength-sized noble particles (e.g., both Au and Ag) show a pronounced SPR effect, resulting in optical properties that remarkably differ from those of their bulk (Jiang et al., 2011). Fig. 7 depicts the surface modification of the LSPR biosensor with antibody on triangle-shaped silver NPs. The prominent advantage of this strategy is that monolayers can be formed, but it also suffers from weak surface regeneration because the Au-S or Ag-S bond is insufficiently strong to resist tough elution conditions.

Graphene generally functions as an enhanced substrate during the construction of optical biosensing devices because of the following advantages (Zeng et al., 2015): (i) Graphene exhibits relatively huge surface area (~2630 m^2/g), hence allowing it to provide enough surface contact with target; (ii) Graphene can induce a greatly improved EM enhancement at the interface of substrate; (iii) The surface of graphene can selectively bind to aromatic compounds via π-stacking force. In general, the graphene surface can be modified for the controllable functionalization of the receptor probe in two ways (Singh et al., 2015). One way is to immobilize the surface with a layer of functional polypyrrole film, while the other is to use pyrene derivatives for non-covalent functionalization where the layer of pyrene is strengthened by electropolymerization. Fig. 8 demonstrates an example of using nitrilotriacetic acid (NTA) group-tethered pyrene and polypyrrole groups to immobilize the biotin-tagged bioreceptor by electropolymerization.

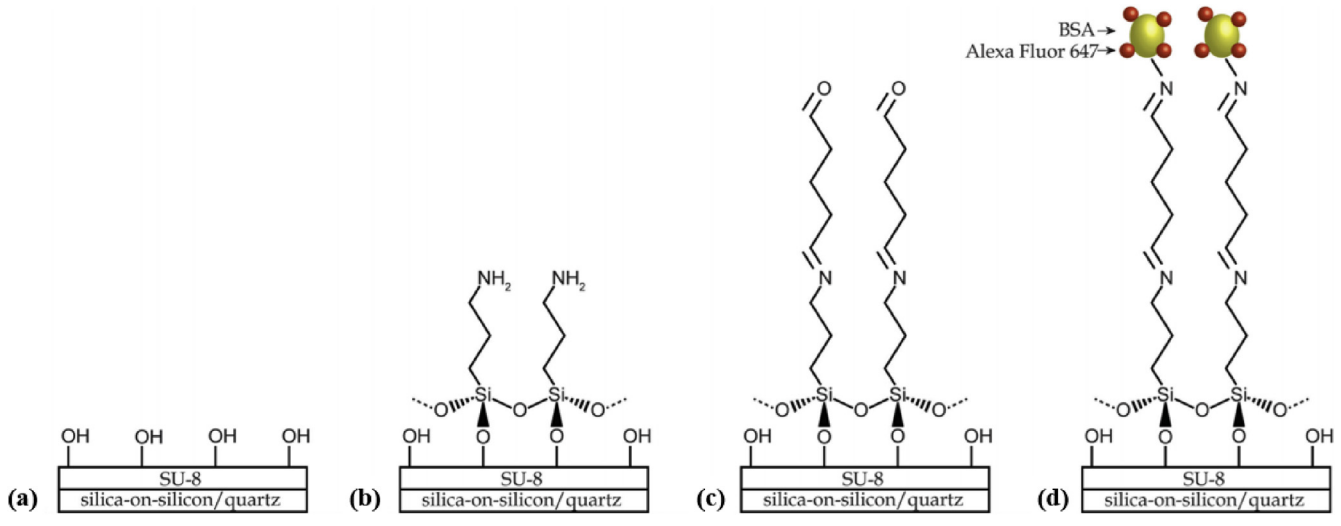

Fig. 6. Illustration of surface functionalization of SU-8 materials: **(a)** generation of hydroxyl groups; **(b)** silanization; **(c)** reaction with glutaraldehyde; **(d)** BSA-Alexa 647 immobilization (reprinted from Ref (Abdul-Hadi et al., 2018). with permission).

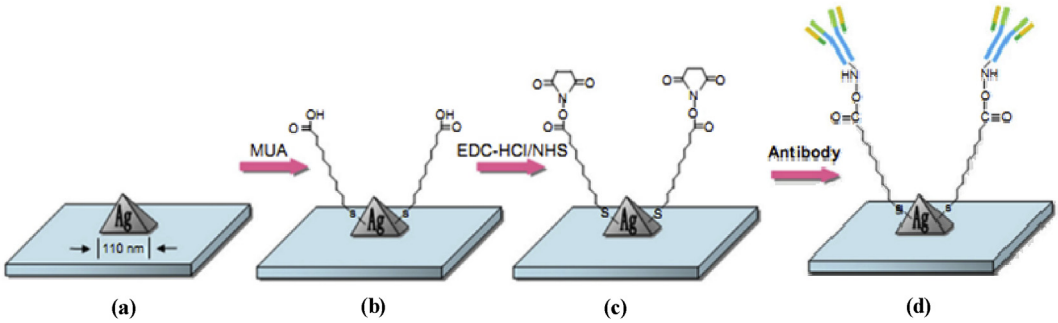

Fig. 7. Illustration of surface functionalization of the LSPR-based biosensor with antibodies. **(a)** the triangle-shaped silver (Ag) NPs-deposited silica substrate. **(b)** SAM generated by incubating with 1 mM MUA. **(c)** Further incubation in 75 mM EDC-HCl/15 mM NHS solution. **(d)** Immobilization of antibodies (with a slight modification from Ref (Zhao et al., 2014)).

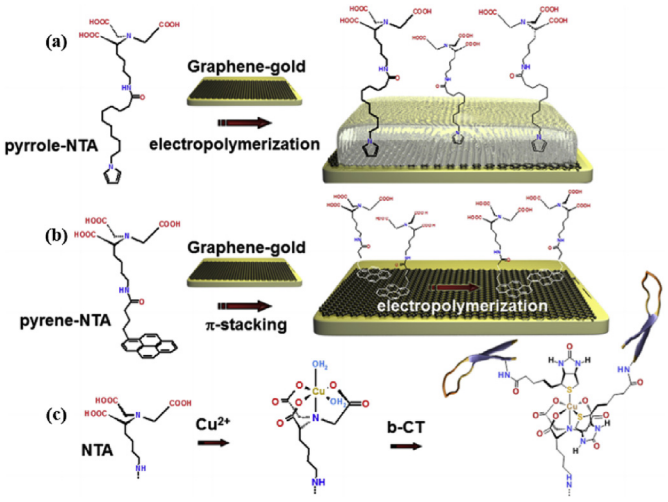

Fig. 8. Illustration of surface functionalization of a graphene layer, including **(a)** immobilization of a polypyrrole-NTA layer by electropolymerization and **(b)** further π-stacking of pyrene-NTA to reinforce the layer. **(c)** Schemes of the conditioning reactions of the NTA group for the purpose of immobilizing b-CT (with a slight modification from Ref (Singh et al., 2015)).

4. Applications

LoD and specificity (also known as selectivity) are the key factors in determining the practicality of biosensors in real applications, especially when faced with complex environmental and clinical matrices. LoD towards target is the more important parameter to characterize the complete biosensor. It needs to be decreased so that low concentrations can be detected ensuring early detection of disease or of pollutants, for example, and it can be achieved by (i) improving sensitivity of optical device, (ii) improving surface functionalization quality or (iii) reducing system noise and drift. On the premise of rejecting non-specific interferences to the greatest extent, the specificity of a biosensor depends largely on the inside nature characteristics of biorecognition elements, and varies widely with the screening strategies and conditions from case to case and, therefore, is not discussed here. Most optical biosensors based on the refractometric sensing scheme are still in the stage of infancy with the exception of the SPR biosensor. For these biosensors, efforts are dedicated to device improvement and optimization. However, downstream practical applications are still expected. Thus, this part of the paper will focus on recent advances in various sensing strategy cases designed for potential applications in view of the diverse recognition elements (enzyme, antibody, nucleic acid, receptor and whole cell).

4.1. Enzyme-based detection

Enzymes are proteins that can catalyze specific chemical reactions in purified states or existing in a slice of tissue or a microorganism. Baliyan et al. (2016) established a label-free biosensor using long period fiber grating (LPG) to quantitatively measure the triacylglyceride concentration by covalently immobilizing the lipase enzyme directly on the surface of LPG. The change in the resonance wavelength of the transmission spectra, generated by the lipase enzyme-immobilized LPG, could be used to acquire the triacylglyceride concentrations. The sensitivity of this sensor was as high as 0.5 nm/mM with a low LoD of 17.71 mg/dL for triacylglycerides in human blood within physiological range. Arjmand et al. (2017) constructed a label-free biosensor on the basis of a non-adiabatic tapered fiber, which was operated based on the interference of propagation modes to detect methyl-parathion (MPT, an organophosphate pesticide) by online monitoring of the binding of MPT to acetylcholinesterase immobilized on the fiber probe. The working range of the sensor for MPT detection was from 10^{-10} to 5×10^{-5} mol/L with a LoD of 2.4×10^{-10} mol/L. However, less enzyme-based optical biosensors have been reported compared with similar kind of electrochemical biosensors considering that the electron transfer is the essence of enzymatic reactions.

4.2. Antibody-based detection

Antibodies, as the most-established affinity recognition elements, have been widely utilized in the fields such as clinics, environmental monitoring, food safety and biotechnology (Hu et al., 2014b; Lee et al., 2012; Feng et al., 2017). To date, immunoassays are the most well-established systems employed in refractometric sensing optical biosensors. Several sensing schemes are utilized (Benito-Pena et al., 2016): (i) direct, (ii) sandwich and (iii) competitive immunoassays. Representative examples of antibody-based refractometric sensing optical biosensors are summarized in terms of sensor type, sensing scheme, target, LoD and reference source in Table 1.

4.3. Nucleic acid-based detection

The typical transduction used in such biosensors needs the immobilization of a single-stranded oligonucleotide sequence on the optical transducer surface for capturing the target of interest to produce detectable optical signals. Similar as the label free immunosensors, nucleic acids-based biosensors can be performed by the same sensing schemes (e.g. direct, competitive, and sandwich assay formats) to transduce the recognition process. Representative examples of nucleic acids-based refractometric sensing optical biosensors are summarized in terms of sensor type, sensing schemes, target, LoD and reference source in Table 2.

Table 1
Applications of antibody-based refractometric sensing optical biosensors.

Sensor type	Scheme	Target	LoD	Ref
MZI	Direct	C-reactive protein	2.1 ng/mL	Psarouli et al. (2017)
MZI	Direct	anti-IgG	27 ng/mL	Chen et al. (2013)
MZI	Direct	anti-IgG	1 ng/mL	Shew et al. (2008)
YI	Direct	HSV-1 Virus	850 copies/mL	Ymeti et al. (2007)
SPR	Direct	hCG	106 ng/mL	Soler et al. (2014)
		FAK	86 ng/mL	
		CRP	23 ng/mL	
SPR	Direct	Ischemia-modified albumin	0.01 ng/mL	Li et al. (2013)
SPR	Direct	*Salmonella Typhimurium*	10^4 cfu/mL	Farka et al. (2016)
SPR	Direct	H7N9 virus	144 copies/mL	Chang et al. (2018)
SPR	Competitive	Ractopamine	0.12 ng/mL	Liu et al. (2012)
SPRi	Direct	*Salmonella enterica*	1 cfu/mL	Templier et al. (2017)
SPRi	Competitive	Clenbuterol	6.32×10^3 ng/mL	Yao et al. (2015)
SPRi	Indirect	Adenoviruses	10 PFU/mL	Abadian et al. (2015)
SPRi	Sandwich	KIM-1	5×10^{-3} ng/mL	Zeidan et al. (2016)
		HMGB-1		
SPRi	Sandwich	Carcinoembryonic antigen	0.5 ng/mL	Hu et al. (2014b)
SPRi	Sandwich	α-fetoprotein	1 ng/mL	Hu et al. (2014a)
LSPR	Direct	Alzheimer's tau protein	10 ng/mL	Vestergaard et al. (2008)
LSPR	Direct	Cytokine	2.5×10^{-4} ng/mL	Park et al. (2017b)
LSPR	Direct	Digoxin	2 ng/mL	Nikfarjam et al. (2017)
LSPR	Direct	Free prostate specific antigen	1×10^{-4} ng/mL	Sanders et al. (2014)
LSPR	Direct	HIV-1	2×10^{-4} ng/mL	Lee et al. (2013)
LSPR	Sandwich	Cytochrome-c	0.1 ng/mL	Loo et al. (2017)
LRSPR	Sandwich	BSA	10 ng/mL	Khodami and Berini (2018)
Ring resonator	Competitive	2,4-dichlorophenoxyacetic acid	4.5 ng/mL	Feng et al. (2017)
Ring resonator	Direct	Prostate specific antigen	0.1 ng/mL	Lee et al. (2012)
Ring resonator	Direct	Carcinoembryonic antigen	2 ng/mL	(Washburn et al., 2009)
Ring resonator	Sandwich	Human cytokine interleukin-2	0.1 ng/mL	Luchansky and Bailey (2010)
Photonic crystal	Direct	Angiopoietin-1	0.4 ng/mL	Frascella et al. (2016)
Photonic crystal	Direct	Cardiac troponin I	0.1 ng/mL	Zhang et al. (2014)

4.4. Whole cell-based detection

Utilization of live whole cells rather than isolated biological ingredients to develop biosensors exhibits some advantages such as high tolerance to pH or temperature changes. A single cell contains almost all the enzymes and co-factors required for detection of the targets; measurement is usually feasible without the massive sample preparation and the biosensors can be well regenerated by cell rebirth. The function of an olfactory receptor, ODR-10, in a living heterologous cell system of HEK-293 by using the SPR technique was demonstrated (Lee et al., 2006). The HEK-293 cells were stably cultivated on the gold SPR chip surface coated with poly-d-lysine, while the ODR-10 was excreted by the HEK-293 cells, which could specifically bind to an odorant molecule, diacetyl. As a result, a SPR signal was observed when the HEK-293 cells exposed to diacetyl due to the binding event between diacetyl and ODR-10, and the signal intensity was dependent on the exposure dose of diacetyl. More cell-based SPR biosensors have been summarized in a relevant review, especially for their applications in clinic (Yanase et al., 2014).

Table 2
Applications of nucleic acid-based refractometric sensing optical biosensors.

Sensor type	Scheme	Target	LoD	Ref
MZI	Direct assay	*Methicillin-resistant staphylococcus aureus* specific DNA	0.4 nM	Melnik et al. (2016)
YI	Direct assay	ssDNA	50 nM	Hradetzky et al. (2006)
SPR	Direct assay	MicroRNA	4.5×10^{-5} nM	Hao et al. (2017)
SPR	Direct assay	Tetracycline	6.9 ng/kg	Wang et al. (2018b)
SPR	Direct assay	*Mycobacterium* DNA	2.6×10^{-4} nM	Silvestri et al. (2015)
SPR	Direct assay	Staphylococcal Enterotoxin B	2×10^4 ng/mL	Dudak and Boyaci (2014)
SPR	Direct assay	Aflatoxin B_1	0.12 ng/mL	Sun et al. (2017)
SPR	Direct assay	IgE	3.44 ng/mL	Kim et al. (2009)
	Sandwich assay		2.07 ng/mL	
SPR	Sandwich assay	Tetracycline	4.44×10^{-9} ng/mL	Kim and Lee (2017)
SPR	Hemin/G-quadruplex	Pb^{2+}	1×10^{-6} ng/mL	Pelossof et al. (2012)
SPR	Dynamic and structural DNA nanodevices	HIV-related DNA	4.8×10^{-5} nM	Diao et al. (2018)
SPRi	Direct assay	BCR/ABL fusion gene	10.29 nM	Wu et al. (2016)
SPRi	Sandwich assay	MicroRNA	5×10^{-4} nM	Vaisocherova et al. (2015)
LSPR	Direct assay	Tumor necrosis factor DNA	0.677 nM	Endo et al. (2005)
LSPR	Direct assay	MicroRNA	5×10^{-3} nM	Zhang et al. (2017a)
LSPR	Sandwich assay	Ochratoxin A	2.26×10^{-4} ng/mL	Park et al. (2017a)
		Adenosine triphosphate	4.41×10^{-4} ng/mL	
		Aflatoxin B1	1.96×10^{-4} ng/mL	
		Potassium ions	4.12×10^{-5} ng/mL	
LSPR	Direct assay	Tobramycin	2.33×10^2 ng/mL	Cappi et al. (2015)

4.5. Others

Arya et al. (2011) developed a SPR biosensor to detect *Escherichia coli* K12 bacteria by covalently immobilizing a T4 bacteriophage as a bioreceptor on gold chip surface, exhibiting the dynamic detection range of 7×10^2–7×10^8 cfu/mL. However, the drying of surface-immobilized whole phages heavily impaired their capture efficiency. Furthermore, the overexposure to the phages might cause the lysis and possible ruin of the captured pathogen. Thus, a receptor binding protein, i.e. *Campylobacter* bacteriophage NCTC 12673, was immobilized rather than a bacteriophage on the gold surface of SPR chip, achieving the specific detection of *Campylobacter jejuni* with a LoD of 100 cfu/mL (Singh et al., 2011). The multivalent protein-carbohydrate (lectin) was utilized as a specific recognition element to selectively detect *Candida albicans* with a LoD of 32 cfu/mL by using the SPR technique (Cai et al., 2015). An SPR biosensor used a phenylboronic acid derivative as a receptor molecule, which was immobilized on the chip sensing area to measure glycoprotein with an LoD of 1.556×10^{-8} M (Zhang et al., 2017b).

Artificial receptors, such as molecular imprinting polymers (MIPs) generated by molecular imprinting, can bind a target molecule with comparable sensitivity and selectivity to their natural counterparts yet present excellent stability, low cost and good reproducibility (Ye and Haupt, 2004). A MIP-based biomimetic SPR sensor by using a tapered plastic optical fiber as transducer was reported for the detection of l-nicotine with a linearity range of 0–10^{-3} M; moreover, measurement was possibly lasting over a period of at least 2 months (Cennamo et al., 2014). A biomimetic SPR sensor was described using a MIP via covalent coupling for the detection of the drug, exhibiting a LoD of 1.9×10^{-9} g/mL towards metoprolol (Altintas et al., 2016). Unfortunately, the efficient integration of MIPs with a label-free optical transducer is still one of the major bottleneck problems for the development of MIP-based biosensor.

5. Summary and conclusions

Optical biosensors based on refractometric sensing schemes, such as interferometer-, SPR-, WGM-, and PC-based biosensors, are reviewed with their sensing principles, structural design, and integration improvements. Among such optical biosensors, interferometric-based biosensors are the earliest and simplest structures from fabrication to integration. However, they lack flexibility of multiplexed detection and frequently are criticized for their insufficient sensitivity. SPR-based biosensors are the most maturely established with relatively high sensitivity. CCD detection promotes the SPRi technique with high-throughput detection capability. The high NA oil microscope used as coupling instrument greatly improves the high resolution compared with conventional SPR, thereby even achieving single particle detection. Emerging complementary metal oxide semiconductor processes and nanomaterials have facilitated the scalable and reliable fabrication of sensing devices at micro- and nanoscale, which promotes the development of SPRi and LSPR with advantages of integrated configuration, improved sensitivity and high-throughput multiplexed detection capability. Optical WGM microcavities with high quality factors that restrict light into a small volume significantly enhance the interaction between target and light for a wide variety of biomolecules sensing applications. And PC-based biosensors combine structures, such as microcavities and waveguides, with new materials to realize the biosensing with ultra-compact size and excellent sensitivity. These types of sensors are explored for POC applications through integration with emerging technologies such as smartphones and flexible and wearable materials.

6. Future prospectives

Looking to the future, the development of novel materials, hybrid materials, nanomaterials and novel fabrication techniques of micro/nanostructures to enhance optical intensity confinement for strong light-target interaction should be continuously beneficial to improve the sensitivity and signal-to-noise ratio, and hence decreasing the LoD of the sensing devices. For example, the emergence of graphene in combination with plasmonic metal NPs is attaining much attention to form improved LSPR biosensing system (Chiu et al., 2018; Ng et al., 2017). Screening of optimal microcavity materials and geometries enables change in light confinement and the investigation of nonlinearities to achieve a maximal figure of merit (FOM, defined as sensitivity divided by the resonant bandwidth by Sherry et al., 2005) (Xavier et al., 2018). Fano resonances, which can be tuned by depositing single plasmonic nanoparticles on top of the transition metal dichalcogenide monolayers like WS_2 (Wang et al., 2018a) and WSe_2 (Sun et al., 2018) exhibit sharp and asymmetric spectral line-shapes and strong field enhancements (Wang et al., 2019). These hybrid systems will pave new pathways to develop more sensitive refractometric biosensing systems. Microfluidic-based research, driven by the promise of miniaturization and integration of complex biosensing steps, has successfully transformed a high-throughput, label-free, multi-arrayed LSPR optical biosensor to the submillimeter scale (Chen et al., 2015a). Although different parameters have been used to characterize and compare the performance of refractometric sensing-based optical devices, such as sensitivity to RI change and FOM (Xavier et al., 2018; Xu et al., 2019), it cannot be ignored that the LoD of a biosensor towards a biochemical target also depends very strongly on the sensitivity and specificity of the biorecognition element and the accuracy of the surface functionalization (Vollmer and Yang, 2012). Combining the smartphone with the refractometric sensing biosensors is still a trend, which shows great potential for the development of network-based sensing with a variety of down-stream applications, for example the smartphone-combined SPR biosensor (Liu et al., 2015b), SPRi biosensor (Guner et al., 2017), and LSPR biosensor (Dutta et al., 2016) for POC, environmental monitoring and food safety. Novel sensing mechanisms are still needed to be further exploited. In short, breakthroughs in physics, chemistry, microfabrication and electronics, materials, nanotechnology and biotechnology have accelerated and deepened our understanding the fundamental physicochemical properties of optical biosensing devices in recent decades. The gap between scientific advances and real downstream applications in a wide range of fields is gradually being closed.

CRediT authorship contribution statement

Yangyang Chen: Writing - original draft, Visualization, Writing - review & editing. **Jinchuan Liu:** Writing - original draft, Visualization, Writing - review & editing. **Zhenchuan Yang:** Writing - review & editing. **James S. Wilkinson:** Conceptualization, Methodology, Writing - original draft, Supervision, Writing - review & editing, Visualization, Funding acquisition. **Xiaohong Zhou:** Conceptualization, Methodology, Writing - original draft, Supervision, Writing - review & editing, Visualization, Funding acquisition.

Declaration of competing interest

The authors declare that they have no known competing financial interests or personal relationships that could have appeared to influence the work reported in this paper.

Acknowledgements

This research is supported by Beijing Municipal Natural Science Foundation-Haidian Primitive Innovation Joint Fund Project (L182045) and the Royal Society-China NSFC-Newton Mobility Grant (IE161436).

Appendix A. Supplementary data

Supplementary data to this article can be found online at https://doi.org/10.1016/j.bios.2019.111693.

References

Abadian, P.N., Yildirim, N., Gu, A.Z., Goluch, E.D., 2015. Biosens. Bioelectron. 74, 808–814.
Abdul-Hadi, J., Gauthier, M.A., Packirisamy, M., 2018. IEEE Photonics Journal 10 (6), 1–15.
Altintas, Z., France, B., Ortiz, J.O., Tothill, I.E., 2016. Sens. Actuators B Chem. 224, 726–737.
Arjmand, M., Saghafifar, H., Alijanianzadeh, M., Soltanolkotabi, M., 2017. Sens. Actuators B Chem. 249, 523–532.
Arya, S.K., Singh, A., Naidoo, R., Wu, P., McDermott, M.T., Evoy, S., 2011. Analyst 136 (3), 486–492.
Baaske, M.D., Foreman, M.R., Vollmer, F., 2014. Nat. Nanotechnol. 9 (11), 933–939.
Baliyan, A., Sital, S., Tiwari, U., Gupta, R., Sharma, E.K., 2016. Biosens. Bioelectron. 79, 693–700.
Bañuls, M.-J., Puchades, R., Maquieira, Á., 2013. Anal. Chim. Acta 777, 1–16.
Benito-Pena, E., Valdes, M.G., Glahn-Martinez, B., Moreno-Bondi, M.C., 2016. Anal. Chim. Acta 943, 17–40.
Blaszykowski, C., Sheikh, S., Thompson, M., 2012. Chem. Soc. Rev. 41 (17), 5599–5612.
Brandenburg, A., Krauter, R., Künzel, C., Stefan, M., Schulte, H., 2000. Appl. Opt. 39 (34), 6396–6405.
Cai, Z.Y., Kwak, D.H., Punihaole, D., Hong, Z.M., Velankar, S.S., Liu, X.Y., Asher, S.A., 2015. Angew. Chem. Int. Ed. 54 (44), 13036–13040.
Cappi, G., Spiga, F.M., Moncada, Y., Ferretti, A., Beyeler, M., Bianchessi, M., Decosterd, L., Buclin, T., Guiducci, C., 2015. Anal. Chem. 87 (10), 5278–5285.
Caucheteur, C., Guo, T., Albert, J., 2015. Anal. Bioanal. Chem. 407 (14), 3883–3897.
Cennamo, N., D'Agostino, G., Pesavento, M., Zeni, L., 2014. Sens. Actuators B Chem. 191, 529–536.
Chang, Y.F., Wang, W.H., Hong, Y.W., Yuan, R.Y., Chen, K.H., Huang, Y.W., Lu, P.L., Chen, Y.H., Chen, Y.M.A., Su, L.C., Wang, S.F., 2018. Anal. Chem. 90 (3), 1861–1869.
Chen, L.H., Chan, C.C., Ni, K., Hu, P.B., Li, T., Wong, W.C., Balamurali, P., Menon, R., Shaillender, M., Neu, B., Poh, C.L., Dong, X.Y., Ang, X.M., Zu, P., Tou, Z.Q., Leong, K.C., 2013. Sens. Actuators B Chem. 178, 176–184.
Chen, P., Chung, M.T., McHugh, W., Nidetz, R., Li, Y., Fu, J., Cornell, T.T., Shanley, T.P., Kurabayashi, K., 2015a. ACS Nano 9, 4173–4181.
Chen, Y., Yu, F., Yang, C., Song, J., Tang, L., Li, M., He, J.-J., 2015b. Opt. Commun. 344, 129–133.
Chiu, N.-F., Chen, C.-C., Yang, C.-D., Kao, Y.-S., Wu, W.-R., 2018. Nanoscale Res. Lett. 13 (1), 152.
Claes, T., Molera, J.G., De Vos, K., Schacht, E., Baets, R., Bienstman, P., 2009. IEEE Photonics J 1 (3), 197–204.
Claes, T., Bogaerts, W., Bienstman, P., 2010. Opt. Express 18 (22), 22747–22761.
Csaki, A., Stranik, O., Fritzsche, W., 2018. Expert Rev. Mol. Diagn. 18 (3), 279–296.
Culver, H.R., Wechsler, M.E., Peppas, N.A., 2018. ACS Nano 12 (9), 9342–9354.
Cunningham, B.T., Laing, L., 2006. Expert Rev. Proteomics 3 (3), 271–281.
Damborský, P., Švitel, J., Katrlík, J., 2016. Opt. biosen. Essays In Biochemistry 60 (1), 91.
Diao, W., Tang, M., Ding, S.J., Li, X.M., Cheng, W.B., Mo, F., Yan, X.Y., Ma, H.M., Yan, Y.R., 2018. Biosens. Bioelectron. 100, 228–234.
Dudak, F.C., Boyaci, I.H., 2014. Food Anal. Method 7 (2), 506–511.
Dutta, S., Saikia, K., Nath, P., 2016. RSC Adv. 6 (26), 21871–21880.
Duval, D., Lechuga, L.M., 2015. In: Andrews, D.L. (Ed.), Photonics: Scientific Foundations, Technology and Applications, IV, pp. 323–365 USA.
Endo, T., Kerman, K., Nagatani, N., Takamura, Y., Tamiya, E., 2005. Anal. Chem. 77 (21), 6976–6984.
Farka, Z., Jurik, T., Pastucha, M., Skladal, P., 2016. Anal. Chem. 88 (23), 11830–11836.
Feng, X.L., Zhang, G., Chin, L.K., Liu, A.Q., Liedberg, B., 2017. ACS Sens. 2 (7), 955–960.
Fenzl, C., Hirsch, T., Wolfbeis, O.S., 2014. Angew. Chem., Int. Ed. Engl. 53 (13), 3318–3335.
Flueckiger, J., Schmidt, S., Donzella, V., Sherwali, A., Ratner, D.M., Chrostowski, L., Cheung, K.C., 2016. Opt. Express 24 (14), 15672–15686.
Foreman, M.R., Swaim, J.D., Vollmer, F., 2015. Adv. Opt. Photon 7 (2), 168–240.
Frascella, F., Petri, C., Ricciardi, S., Napione, L., Munzert, P., Jonas, U., Dostalek, J., Bussolino, F., Pirri, C.F., Descrovi, E., 2016. J. Lightwave Technol. 34 (15), 3641–3645.
Gorodetsky, M.L., Savchenkov, A.A., Ilchenko, V.S., 1996. Opt. Lett. 21 (7), 453–455.
Gunda, N.S.K., Singh, M., Norman, L., Kaur, K., Mitra, S.K., 2014. Appl. Surf. Sci. 305, 522–530.
Guner, H., Ozgur, E., Kokturk, G., Celik, M., Esen, E., Topal, A.E., Ayas, S., Uludag, Y., Elbuken, C., Dana, A., 2017. Sens. Actuators B Chem. 239, 571–577.
Hao, K.H., He, Y., Lu, H.T., Pu, S.T., Zhang, Y.N., Dong, H.F., Zhang, X.J., 2017. Anal. Chim. Acta 954, 114–120.
Heideman, R.G., Kooyman, R.P.H., Greve, J., 1991. Sens. Actuators B Chem. 4 (3), 297–299.
Heideman, R.G., Kooyman, R.P.H., Greve, J., 1993. Sens. Actuators B Chem. 10 (3), 209–217.
Hosseini, S., Ibrahim, F., Djordjevic, I., Koole, L.H., 2014. Analyst 139 (12), 2933–2943.
Hradetzky, D., Mueller, C., Reinecke, H., 2006. J. Opt. A Pure Appl. Opt. 8 (7), S360–S364.
Hu, W.H., Chen, H.M., Shi, Z.Z., Yu, L., 2014a. Anal. Biochem. 453, 16–21.
Hu, W.H., He, G.L., Zhang, H.H., Wu, X.S., Li, J.L., Zhao, Z.L., Qiao, Y., Lu, Z.S., Liu, Y., Li, C.M., 2014b. Anal. Chem. 86 (9), 4488–4493.
Hu, T., Dong, B., Luo, X., Liow, T.-Y., Song, J., Lee, C., Lo, G.-Q., 2017. Photonics Res. 5 (5), 417–430.
Huang, H., He, C., Zeng, Y., Xia, X., Yu, X., Yi, P., Chen, Z., 2009. Biosens. Bioelectron. 24 (7), 2255–2259.
Inan, H., Poyraz, M., Inci, F., Lifson, M.A., Baday, M., Cunningham, B.T., Demirci, U., 2017. Chem. Soc. Rev. 46 (2), 366–388.
Jahns, S., Brau, M., Meyer, B.O., Karrock, T., Gutekunst, S.B., Blohm, L., Selhuber-Unkel, C., Buhmann, R., Nazirizadeh, Y., Gerken, M., 2015. Biomed. Opt. Express 6 (10), 3724–3736.
Jamil, M.M.A., Denyer, M.C.T., Youseffi, M., Britland, S.T., Liu, S., See, C.W., Somekh, M.G., Zhang, J., 2008. J. Struct. Biol. 164 (1), 75–80.
Jayanthi, V.S.P.K., Sankara, A., Das, A.B., Saxena, U., 2017. Biosens. Bioelectron. 91, 15–23.
Jensen, Traci R., Malinsky, M.D., Christy, L., Haynes, a., Duyne, R.P.V., 2000. J. Phys. Chem. B 104 (45), 10549–10556.
Jiang, H.-L., Akita, T., Ishida, T., Haruta, M., Xu, Q., 2011. J. Am. Chem. Soc. 133 (5), 1304–1306.
Kabashin, A.V., Patskovsky, S., Grigorenko, A.N., 2009. Opt. Express 17 (23), 21191–21204.
Khodami, M., Berini, P., 2018. Sens. Actuators B Chem. 273, 1156–1161.
Kim, E., Baaske, M.D., Vollmer, F., 2017. Lab Chip 17 (7), 1190–1205.
Kim, S., Lee, H.J., 2017. Anal. Chem. 89 (12), 6624–6630.
Kim, Y.H., Kim, J.P., Han, S.J., Sim, S.J., 2009. Sens. Actuators B Chem. 139 (2), 471–475.
Kozma, P., Kehl, F., Ehrentreich-Förster, E., Stamm, C., Bier, F.F., 2014. Biosens. Bioelectron. 58, 287–307.
Lee, J.Y., Ko, H.J., Lee, S.H., Park, T.H., 2006. Enzym. Microb. Technol. 39 (3), 375–380.
Lee, H.J., Lee, J.H., Moon, H.S., Jang, I.S., Choi, J.S., Yook, J.G., Jung, H.I., 2012. Sens. Actuators B Chem. 169, 26–31.
Lee, J.H., Kim, B.C., Oh, B.K., Choi, J.W., 2013. Nanomed-Nanotechnol. 9 (7), 1018–1026.
Lee, B., Park, J.-H., Byun, J.-Y., Kim, J.H., Kim, M.-G., 2018. Biosens. Bioelectron. 102, 504–509.
Li, G., Li, X., Yang, M., Chen, M.M., Chen, L.C., Xiong, X.L., 2013. Sensors 13 (10), 12794–12803.
Link, S., El-Sayed, M.A., 1999. J. Phys. Chem. B 103 (40), 8410–8426.
Liu, Y., Li, C.M., 2012. Anal. Lett. 45 (2–3), 130–155.
Liu, M., Ning, B.A., Qu, L.J., Peng, Y., Dong, J.W., Gao, N., Liu, L., Gao, Z.X., 2012. Sens. Actuators B Chem. 161 (1), 124–130.
Liu, Q., Tu, X., Kim, K.W., Kee, J.S., Shin, Y., Han, K., Yoon, Y.-J., Lo, G.-Q., Park, M.K., 2013. Sens. Actuators B Chem. 188, 681–688.
Liu, Q., Shin, Y., Sheng Kee, J., Kim, K.W., Rafeah Mohamed Rafei, S., Perera, P., Tu, X., Lo, G.-Q., Ricci, E., Colombel, M., Chiong, E., Thiery, J., Kyoung Park, M., 2015a. Biosens. Bioelectron. 71, 365–372.
Liu, Y., Liu, Q., Chen, S., Cheng, F., Wang, H., Peng, W., 2015b. Sci. Rep. 5, 12864.
Liu, C., Hu, F., Yang, W., Xu, J., Chen, Y., 2017. Trac. Trends Anal. Chem. 97, 354–362.
Loo, J.F.C., Lau, P.M., Kong, S.K., Ho, H.P., 2017. Micromachines 8 (11), 338.
Luchansky, M.S., Bailey, R.C., 2010. Anal. Chem. 82 (5), 1975–1981.
Luo, Q., Li, X., Gu, Y., Tang, Y., Chen, Y., Yu, F., Yang, C., Li, M., Tang, L., Song, J., He, J.-J., 2014. Proc. SPIE 9268, 926829.
Mayer, K.M., Hafner, J.H., 2011. Chem. Rev. 111 (6), 3828–3857.
Melnik, E., Bruck, R., Hainberger, R., Lammerhofer, M., 2011. Anal. Chim. Acta 699 (2), 206–215.
Melnik, E., Muellner, P., Mutinati, G.C., Koppitsch, G., Schrank, F., Hainberger, R., Laemmerhofer, M., 2016. Sens. Actuators B Chem. 236, 1061–1068.
Mohammadzadeh-Asl, S., Keshtkar, A., Ezzati, N.D.J., De, l.G.M., 2018. Biosens. Bioelectron. 110, 118–131.
Ng, S.P., Qiu, G., Ding, N., Lu, X., Wu, C.-M.L., 2017. Biosens. Bioelectron. 89, 468–476.
Nikfarjam, A., Rezayan, A.H., Mohammadkhani, G., Mohammadnejad, J., 2017. Plasmonics 12 (1), 157–164.
Nordin, A., 2016. Nanobiosensors Dis. Diagnosis 5, 41–50.
Notomi, M., 2011. IEEE 99 (10), 1768–1779.
Park, J.H., Byun, J.Y., Jang, H., Hong, D., Kim, M.G., 2017a. Biosens. Bioelectron. 97, 292–298.
Park, Y., Ryu, B., Oh, B.R., Song, Y.J., Liang, X.G., Kurabayashi, K., 2017b. ACS Nano 11 (6), 5697–5705.
Pelossof, G., Tel-Vered, R., Willner, I., 2012. Anal. Chem. 84 (8), 3703–3709.
Piliarik, M., Bocková, M., Homola, J., 2010. Biosens. Bioelectron. 26 (4), 1656–1661.
Psarouli, A., Botsialas, A., Salapatas, A., Stefanitsis, G., Nikita, D., Jobst, G., Chaniotakis, N., Goustouridis, D., Makarona, E., Petrou, P.S., Raptis, I., Misiakos, K., Kakabakos, S.E., 2017. Talanta 165, 458–465.
Rodriguez, G.A., Hu, S., Weiss, S.M., 2015. Opt. Express 23 (6), 7111–7119.
Sadani, K., Nag, P., Mukherji, S., 2019. Biosens. Bioelectron. 134, 90–96.
Sanders, M., Lin, Y.B., Wei, J.J., Bono, T., Lindquist, R.G., 2014. Biosens. Bioelectron. 61, 95–101.
Sherry, L.J., Chang, S.-H., Schatz, G.C., Van Duyne, R.P., Wiley, B.J., Xia, Y., 2005. Nano Lett. 5, 2034–2038.
Shew, B.Y., Cheng, Y.C., Tsai, Y.H., 2008. Sens. Actuators A Phys. 141 (2), 299–306.
Silvestri, D., Sonato, A., Ruffato, G., Meneghello, A., Antognoli, A., Cretaio, E., Dettin, M., Zamuner, A., Casarin, E., Zacco, G., Romanato, F., Morpurgo, M., 2015. Anal. Methods 7 (10), 4173–4180.
Singh, A., Arutyunov, D., McDermott, M.T., Szymanski, C.M., Evoy, S., 2011. Analyst 136 (22), 4780–4786.
Singh, M., Holzinger, M., Tabrizian, M., Winters, S.a., Berner, N.C., Cosnier, S., Duesberg,

G.S., 2015. J. Am. Chem. Soc. 137 (8), 2800–2803.
Skivesen, N., Têtu, A., Kristensen, M., Kjems, J., Frandsen, L.H., Borel, P.I., 2007. Opt. Express 15 (6), 3169–3176.
Soler, M., Estevez, M.C., Alvarez, M., Otte, M.A., Sepulveda, B., Lechuga, L.M., 2014. Sensors 14 (2), 2239–2258.
Su, Y.-w., Wang, W., 2018. Anal. Bioanal. Chem. 410 (17), 3943–3951.
Sun, L.L., Wu, L.Q., Zhao, Q., 2017. Microchim Acta 184 (8), 2605–2610.
Sun, J., Hu, H., Zheng, D., Zhang, D., Deng, Q., Zhang, S., Xu, H., 2018. ACS Nano 12 (10), 10393–10402.
Suzuki, A., Kondoh, J., Matsui, Y., Shiokawa, S., Suzuki, K., 2005. Sens. Actuators B Chem. 106 (1), 383–387.
Svedendahl, M., Chen, S., Dmitriev, A., Käll, M., 2009. Nano Lett. 9 (12), 4428–4433.
Taniguchi, T., Hirowatari, A., Ikeda, T., Fukuyama, M., Amemiya, Y., Kuroda, A., Yokoyama, S., 2016. Opt. Commun. 365, 16–23.
Templier, V., Livache, T., Boisset, S., Maurin, M., Slimani, S., Mathey, R., Roupioz, Y., 2017. Sci. Rep. 7, 9457.
Thomas, J.C., Goronzy, D.P., Serino, A.C., Auluck, H.S., Irving, O.R., Jimenez-Izal, E., Deirmenjian, J.M., Macháček, J., Sautet, P., Alexandrova, A.N., Baše, T., Weiss, P.S., 2018. ACS Nano 12 (3), 2211–2221.
Tosatti, S., Michel, R., Textor, M., Spencer, N., 2002. Langmuir 18 (9), 3537–3548.
Turner, A.P., 2013. Chem. Soc. Rev. 42 (8), 3184–3196.
Vaisocherova, H., Sipova, H., Visova, I., Bockova, M., Springer, T., Ermini, M.L., Song, X., Krejcik, Z., Chrastinova, L., Pastva, O., Pimkova, K., Merkerova, M.D., Dyr, J.E., Homola, J., 2015. Biosens. Bioelectron. 70, 226–231.
Vala, M., Etheridge, S., Roach, J.A., Homola, J., 2009. Sens. Actuators B Chem. 139 (1), 59–63.
Vestergaard, M., Kerman, K., Kim, D.K., Hiep, H.M., Tamiya, E., 2008. Talanta 74 (4), 1038–1042.
Vollmer, F., Yang, L., 2012. Nanophotonics 1 (3–4), 267–291.
Vollmer, F., Arnold, S., Keng, D., 2008. P. Nati. Acad. Sci. 105 (52), 20701–20704.
Wang, Y., 2010. PhD thesis, Johannes Gutenberg-Universität.
Wang, M., Krasnok, A., Zhang, T., Scarabelli, L., Liu, H., Wu, Z., Liz-Marzan, L.M., Terrones, M., Alu, A., Zheng, Y., 2018a. Adv. Mater. 30 (22), e1705779.
Wang, S., Dong, Y., Liang, X., 2018b. Biosens. Bioelectron. 109, 1–7.
Wang, C., Zhang, T., Zhang, Z., Zheng, H., 2019. Opt. Commun. 452, 434–439.
Washburn, A.L., Gunn, L.C., Bailey, R.C., 2009. Anal. Chem. 81, 9499–9506.
Wijaya, E., Lenaerts, C., Maricot, S., Hastanin, J., Habraken, S., Vilcot, J.-P., Boukherroub, R., Szunerits, S., 2011. Curr. Opin. Solid State Mater. Sci. 15 (5), 208–224.
Wu, L., Chu, H.S., Koh, W.S., Li, E.P., 2010. Opt. Express 18 (14), 14395–14400.
Wu, J.L., Huang, Y., Bian, X.T., Li, D.D., Cheng, Q., Ding, S.J., 2016. Opt. Commun. 377, 24–32.
Wu, L., Guo, J., Wang, Q., Lu, S., Dai, X., Xiang, Y., Fan, D., 2017. Sens. Actuators B Chem. 249, 542–548.
Xavier, J., Vincent, S., Meder, F., Vollmera, F., 2018. Nanophotonics 7, 1–38.
Xie, L., Yan, X., Du, Y., 2014. Biosens. Bioelectron. 53, 58–64.
Xu, Y., Bai, P., Zhou, X., Akimov, Y., Png, C.E., Ang, L.-K., Knoll, W., Wu, L., 2019. Adv. Optical Mater. 7, 1801433 2019.
Yan, H., Huang, L., Xu, X., Tang, N., Chakravarty, S., Chen, R.T., 2017. Proc. SPIE 10081, 100810G.
Yanase, Y., Hiragun, T., Ishii, K., Kawaguchi, T., Yanase, T., Kawai, M., Sakamoto, K., Hide, M., 2014. Sensors 14 (3), 4948–4959.
Yao, M.W., Wu, Y.C., Fang, X.Y., Yang, Y.C., Liu, H.J., 2015. Anal. Biochem. 475, 40–43.
Ye, L., Haupt, K., 2004. Anal. Bioanal. Chem. 378 (8), 1887–1897.
Ymeti, A., Greve, J., Lambeck, P.V., Wink, T., van Hovell, S.W.F.M., Beumer, T.A.M., Wijn, R.R., Heideman, R.G., Subramaniam, V., Kanger, J.S., 2007. Nano Lett. 7 (2), 394–397.
Yu, H., Shan, X., Wang, S., Tao, N., 2017. Anal. Chem. 89 (5), 2704–2707.
Yuan, G., Gao, L., Chen, Y., Liu, X., Wang, J., Wang, Z., 2014. Optik – Int. J. Light Electron. Opt. 125 (2), 850–854.
Zeidan, E., Li, S.Q., Zhou, Z.G., Miller, J., Sandros, M.G., 2016. Sci. Rep. 6, 36348.
Zeng, S., Hu, S., Xia, J., Anderson, T., Dinh, X.-Q., Meng, X.-M., Coquet, P., Yong, K.-T., 2015. Sens. Actuators B Chem. 207, 801–810.
Zhang, B.L., Morales, A.W., Peterson, R., Tang, L., Ye, J.Y., 2014. Biosens. Bioelectron. 58, 107–113.
Zhang, L., Wang, J.H., Zhang, J.X., Liu, Y.Q., Wu, L.Z., Shen, J.J., Zhang, Y., Hu, Y.L., Fan, Q.L., Huang, W., Wang, L.H., 2017a. ACS Sens. 2 (10), 1435–1440.
Zhang, Y., Wang, F., Qian, S.Y., Liu, Z.X., Wang, Q., Gu, Y.Y., Wu, Z.L., Jing, Z.G., Sun, C.S., Peng, W., 2017b. Sensors 17 (10), 2259–2267.
Zhang, Y.N., Zhao, Y., Zhou, T., Wu, Q., 2017c. Lab Chip 18 (1), 57–74.
Zhao, Q., Duan, R., Yuan, J., Quan, Y., Yang, H., Xi, M., 2014. Int. J. Nanomed. 9, 1097–1104.
Zhu, X., Wang, R., Zhou, X., Shi, H., 2017. ACS Appl. Mater. Interfaces 9 (31), 25789–25795.